IOP PUBLISHING
IOP FTC
JOURNAL OF PHYSICS D: APPLIED PHYSICS
J. Phys. D: Appl. Phys. **42** (2009) 032004 (5pp)
doi:10.1088/0022-3727/42/3/032004

FAST TRACK COMMUNICATION

Bulk flow modification with horseshoe and serpentine plasma actuators

Subrata Roy and Chin-Cheng Wang

Computational Plasma Dynamics Laboratory and Test Facility, Department of Mechanical and Aerospace Engineering, University of Florida, Gainesville, FL 32611, USA

E-mail: roy@ufl.edu

Received 29 October 2008, in final form 4 December 2008
Published 31 December 2008
Online at stacks.iop.org/JPhysD/42/032004

Abstract
Two different control devices are introduced to modify the boundary layer thickness by plasma induced velocity in the low speed region. These horseshoe and serpentine shaped actuators are surface compliant and have a significant three-dimensional influence on neighbouring flows. A numerical investigation of the quiescent and flow condition demonstrates active electrodynamic actuation of fluid in all three principal (streamwise, crosswise and surface normal) directions altering the boundary layer thickness. Based on the powering scheme of electrodes, these actuators not only induce flow attachment to the work surface but can also extract momentum from an upstream flow injecting it into the bulk fluid. Such designs could be useful for tripping the flow as well as for separation control as needed.

1. Introduction

In recent years, the surface barrier discharge has been successfully used to control low speed boundary layer flows [1–4]. Such a discharge imparts a body force inside the boundary layer of a fluid in the vicinity of an exposed electrode. Examples include mitigation of low speed flow separation on airfoils at a high angle-of-attack and lift increment and/or drag reduction in airfoils and fuselages. Both pulsed dc and ac powered plasma actuators can induce active control of the neighbouring flow dynamics in an instantaneous manner. However, such a control has limited application due to insufficient control of the boundary layer. For example, it will be highly beneficial if we can find an actuator that can penetrate the edge of an essentially two-dimensional boundary layer directly modifying the bulk flow by actively diverting the direction of the injected momentum. Such a modification may allow active tripping of the flow and may thus help in turbulent flow control. Also it will be very useful if we may use the same device to both mitigate the flow separation and instil turbulence by controlling the powering scheme as needed.

To understand the physics of plasma actuators, a set of multiscale multispecie basic investigations of plasma actuation was conducted by Roy and Gaintonde [5]. They demonstrated the model predictions for charge densities, electric field and gas velocity distributions and showed induced wall jets that mimic trends reported in the experimental literature [1–4]. Boeuf *et al* [6] presented a typical 2 species fluid model of the DBD actuator with ions and electrons. They found that the electrohydrodynamic (EHD) force depends on the slope of the applied voltage and the dielectric layer. Pinheiro [7] solved a 5 species two-dimensional model with N_2^+, N_4^+, O_2^+, O_2^- and electron governing equations based on the hydrodynamic model and found that the ponderomotive forces tend to increase whenever the energized electrode width increases relative to the dielectric width. Based on the first-principles analysis using 8 species of air N_2, N_2^+, N, O_2, O_2^+, O, O^- and electrons, Singh and Roy [8] identified a functional relationship between the electric force and electric and geometric control parameters. The magnitude of the approximated force increases with the fourth power of the amplitude of the rf potential. Thus the induced fluid velocity also increases.

The main purpose of this study is to introduce a new set of horseshoe and serpentine shaped plasma actuators on a flat surface and numerically test their influence in bulk flow control using the reduced order force approximation [8]. Figure 1

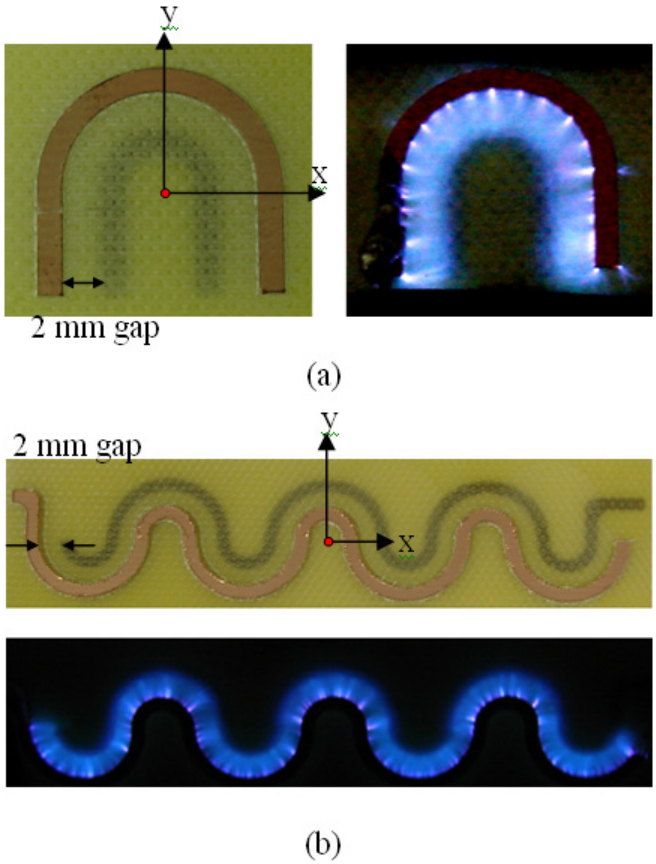

Figure 1. Schematic of the asymmetric single dielectric barrier plasma actuator.

shows the top view of horseshoe and serpentine actuators. It also shows an inward discharge for a horseshoe actuator and a combination of inward and outward discharges for a serpentine actuator. Section 2 gives the details of the computational geometry, the initial and boundary conditions and numerical details. The response to the applied rf potential is described in section 3 for both geometries. Conclusions are drawn in section 4.

2. Problem description

Two types of actuators denoted as horseshoe and serpentine actuators are simulated. Figure 2 shows the schematics of horseshoe and serpentine plasma actuators on the flat plate inside a computational domain. One electrode with red colour is exposed to the fluid, and the other with black is embedded in the dielectric. While both designs have a zero net mass flux, these are unlike circular synthetic jets [4] or circular plasma actuators [9]. Here the electric force from all three planar directions (except from the upstream) pushes the fluid inwards or outwards from the central region. The discharge is generated between the two electrodes shown in figure 1 and changes the flow behaviours by adding momentum to the plasma region. The computational domain is 200 mm long and 100 mm high. The region includes a horseshoe/serpentine plasma actuator consisting of two electrodes separated by a dielectric. In this study, we have only considered the effect of the plasma force

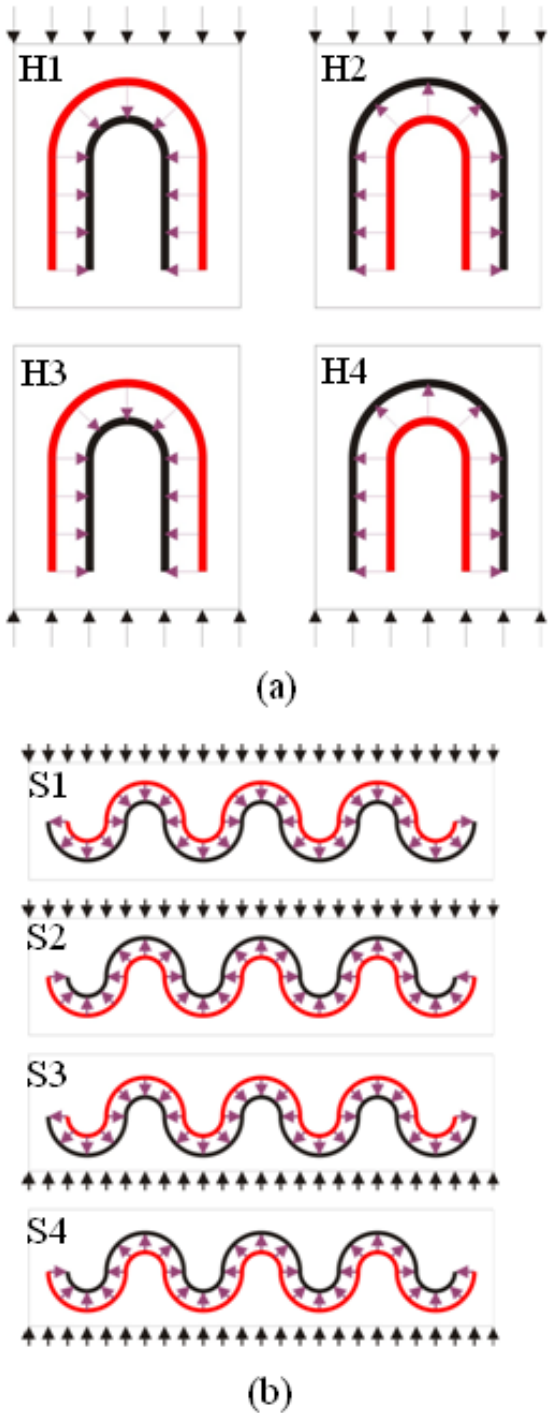

Figure 2. Top view of two schematics for plasma actuation for (*a*) horseshoe and (*b*) serpentine actuators.

in the fluid volume and assumed negligible thickness for the electrodes and the dielectric.

2.1. Horseshoe actuator

The geometry in figure 1(*a*) shows that the powered electrode consists of a half circle with two extended ends in the shape of a horseshoe. The grounded electrode is on the other side of the dielectric with the same shape but smaller. There is a 2 mm horizontal gap between the two electrodes. The origin ($x = y = 0$) is at the centre of the half circle, and the ends of the

half circle extend from $y = 0$ to $y = -7$ mm. We have studied four cases H1–H4 in this paper with different flow directions and polarities shown in figure 2(*a*). For case H1, the inlet flow and inward force are in the same streamwise direction. For case H2, the inlet flow and outward force are in the opposite streamwise direction. For case H3, the inlet flow and inward force are in the opposite streamwise direction. For case H4, the inlet flow and outward force are in the same streamwise direction.

2.2. Serpentine actuator

We modify the horseshoe actuators and connect them one by one, and then they become a serpentine actuator configuration shown in figure 1(*b*). We still keep the 2 mm horizontal gap between the two electrodes. The radius of the small half circle is 2 mm with 2 mm width, and of the big half circle it is 6 mm with 2 mm width. The length from the origin ($x = y = 0$) to one end of the actuator is 38 mm. There are four cases S1–S4 for serpentine actuators with different flow directions and polarities in our studies shown in figure 2(*b*). For case S1, the inlet flow is from the $+y$ axis and the force is a combination of three inward and four outward forces. For case S2, the inlet flow is from the $+y$ axis and the force is a combination of four inward and three outward forces. For case S3, the inlet flow is from the $-y$ axis and the force is a combination of three inward and four outward forces. For case S4, the inlet flow is from the $-y$ axis and the force is a combination of three inward and four outward forces. For both horseshoe and serpentine plasma actuators, we impose the time-averaged body force vector with the purple arrow shown in figure 2. Depending on the actuation device, a local kN m^{-3} force density may be obtained by utilizing a few watts.

We have shown in earlier studies [5, 8] that the electric force ($q\boldsymbol{E}$) is the highest close to the wall surface between the exposed rf electrode and the grounded electrode. With that knowledge and assuming that an essentially time-averaged body force interacts with air, the first principles based electrodynamic force has been approximated by the following equation:

$$\begin{aligned}\boldsymbol{F} = {} & C \times F_{x0} \times \phi_0^4 \times \exp[-((r - r_0 - (z - z_0))/z)^2 \\ & -\beta_x (z - z_0)^2]\hat{i} + C \times F_{y0} \times \phi_0^4 \\ & \times \exp[-((r - r_0 - (z - z_0))/z)^2 - \beta_y (z - z_0)^2]\hat{j} \\ & + C \times F_{z0} \times \phi_0^4 \times \exp[-((r - r_0)/z)^2 - \beta_z (z - z_0)^2]\hat{k}. \end{aligned} \quad (1)$$

Here C is a constant and the values of F_{x0}, F_{y0} and F_{z0} are taken from the average electrodynamic force obtained by solving air-plasma equations. The functional relationship with the fourth power of potential $\phi_0 = 800$ V to the exposed electrode is based on plasma simulation [8] and has been modified for three dimensions. The value of $x_0 = y_0 = r_0 = 0.005$ m is the mid-point between the rf electrode and the grounded electrode, and r_0 is equal to $\sqrt{x_0^2 + y_0^2}$. The value of $z_0 = 0.0001$ m is very close to the flat plate. The values of β_x, β_y and β_z are functions of the dielectric material and are correlated to match the velocity induced by the EHD force. The derivation of the force relation was done using the following boundary conditions for solving first-principles plasma equations: the potential is applied to the exposed electrode with $\phi = \phi_0 \sin(2\pi f t)$ V. The embedded electrode is grounded. The electric insulation condition (normal component of the electric field equal to zero) is assumed at the outer boundaries of the domain. The electric field normal to the dielectric surface is discontinuous by the separated charge. No slip boundary conditions have been applied on the flat plate surface for Navier–Stokes equations. Symmetry boundary conditions have been applied at spanwise boundaries. The first principles numerical details will be given in a following paper.

3. Results and discussion

Nine cases were simulated for this paper. One base case without plasma actuation, four of them related to horseshoe actuator simulation shown in figure 2(*a*) and four cases for serpentine actuator simulation shown in figure 2(*b*). The inlet velocity with a black arrow is acting downwards shown in cases H1, H2, S1 and S2 while it is acting upwards shown in cases H3, H4, S3 and S4. The horseshoe actuator is a combination of half circle and straight line electrodes, so the force vectors with a purple arrow can act inwards (towards the grounded electrode) in cases H1 and H3 or act outwards in cases H2 and H4. The serpentine actuator is a combination of lower and upper parts of half circle electrodes, so the force distribution is acting outwards for the lower part of the half circle and acting inwards for the upper part of the half circle shown in cases S1 and S3 or it is acting in the opposite direction shown in cases S2 and S4. These actuators provide three-dimensional plasma actuation in both streamwise and crosswise directions, and the boundary layer is significantly influenced in the low speed regime by the induced velocity.

3.1. Horseshoe actuator

Figure 3 describes the effect of the imposed (plasma actuator) body force density on a flat plate for different planes. The streamwise velocity V_y for cases H1–H4 on the yz-plane ($x = 0$) show clockwise vortex induced by plasma actuation in cases H1 and H3 and a counterclockwise vortex generated in cases H2 and H4. For cases H1 and H4, we find the highest streamwise velocity very close to the wall. The result shows a decrease in the boundary layer thickness. For case H2, strong plasma actuation which is close to the wall pushes the fluid in streamwise and crosswise directions away from the centreline of the actuator, so there is a stagnation region along the centreline. For case H3, the inward plasma actuation accumulates the fluid towards the centreline of the actuator and pinches the fluid going upwards past this barrier. The result shows a significant tripping resulting in a local increase in the boundary layer thickness.

Figure 4 shows the velocity V_z for cases H1–H4 on the vertical mid-plane ($y = 0$). For cases H1 and H3, there are two vortices generated between the plasma regions, and the velocity V_z at the origin goes upwards because the fluid

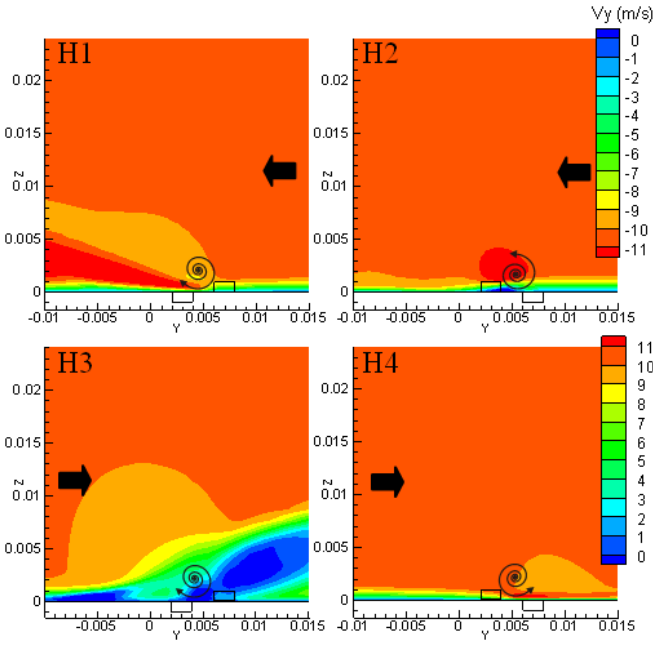

Figure 3. Comparison of streamwise velocity V_y for various configurations for H1–H4 at $x = 0$.

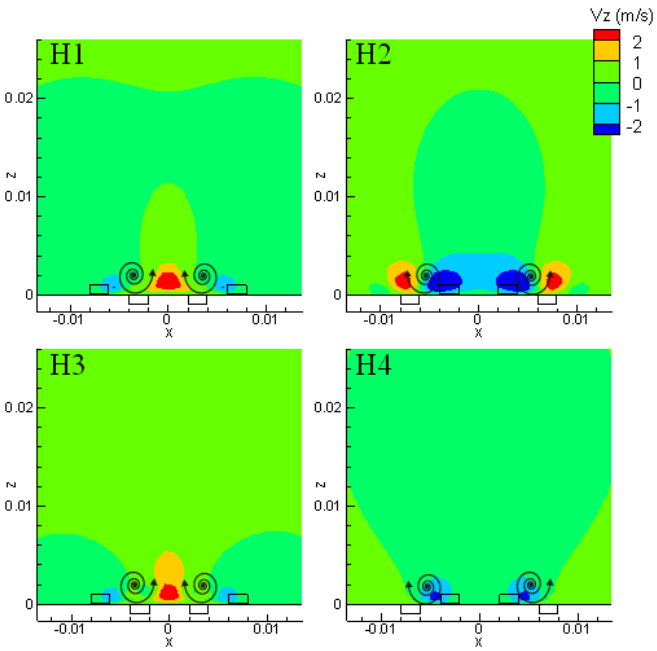

Figure 4. Comparison of upward velocity V_z for various configurations for H1–H4 at $y = 0$.

is drawn inwards by the plasma actuation force between the electrodes. For cases H2 and H4, two vortices are generated by the induced velocity by which the fluid is pulled towards the origin and pushed upwards between the plasma regions. So the results show the highest upward velocity V_z at the origin for cases H1 and H3 and in the plasma region for case H2. There is no upward V_z for case H4 because the fluid attaches to the wall in the plasma region.

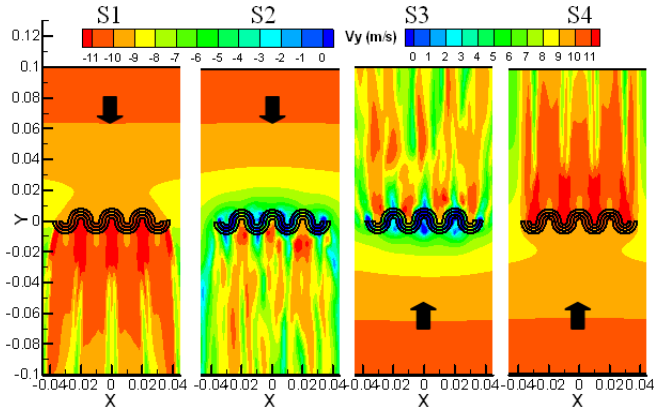

Figure 5. Comparison of streamwise velocity V_y for various configurations for S1–S4 at $z = 1$ mm.

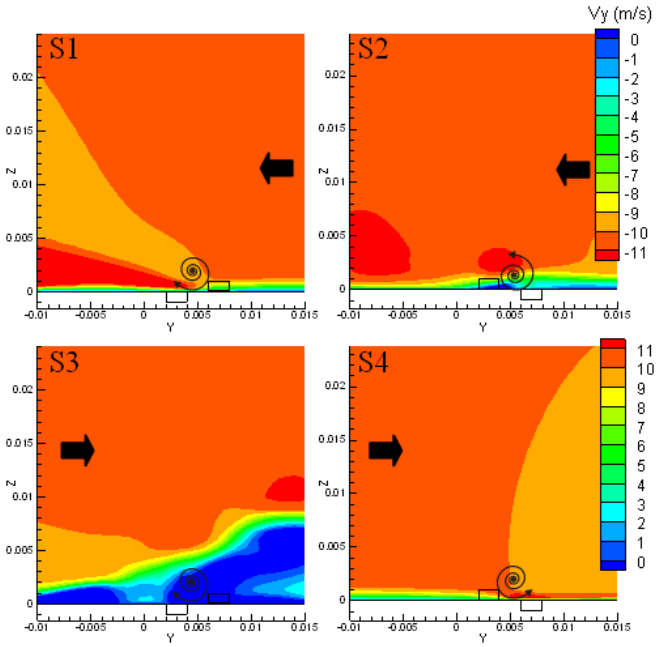

Figure 6. Comparison of streamwise velocity V_y for various configurations for S1–S4 at $x = 0$.

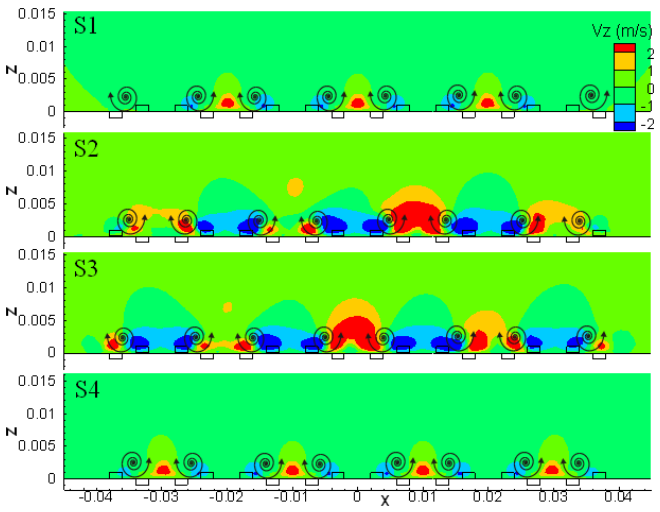

Figure 7. Comparison of upward velocity V_z for various configurations for S1–S4 at $y = 0$.

3.2. Serpentine actuator

Figures 5–7 plot the effect of a serpentine actuator on a flat plate. The streamwise velocity V_y for cases S1–S4 on the *xy*-plane (1 mm above the actuator) in figure 5 shows a very complex pattern of flow. Figure 6 shows the result of the velocity V_y distribution for cases S1–S4 on the *yz*-plane ($x = 0$). The results of cases S1 and S2 are similar to cases H1 and H2 shown in figure 3 due to the same plasma actuation and flow directions interacting with the fluid at the centreline of the actuator. For case S3, the boundary layer thickness is higher than case H3 shown in figure 3 because the curve electrodes induce velocity in the streamwise and crosswise directions rather than only in the crosswise direction for the straight line electrodes. For case S4, we find that the highest streamwise velocity attaches to the downstream surface of the actuator due to the outward plasma actuation.

Figure 7 shows the upward velocity V_z for cases S1–S4 on the vertical mid-plane ($y = 0$). We find that vortices pairs appear between the two electrodes. Cases S1 and S4 show a very similar result of the V_z velocity because of the same streamwise direction for force and fluid flow directions. For case S2, the inward plasma actuation pinches the fluid, so the fluid has to pass the blocking in four plasma regions and shows the highest upward velocity. The same situation occurs in case S3 for three plasma regions.

4. Conclusion

Two new (horseshoe and serpentine) designs of the plasma actuators were introduced. Numerical simulation of these actuators predicts full three-dimensional control unlike the traditional actuators reported thus far. The documented results for several electrical and geometric arrangements show active modification of the boundary layer thickness suitable for tripping and flow attachment using the same actuator. Realistic PIV experimentation is underway to validate the flow behaviours for these designs.

Acknowledgment

This work was partially supported by AFOSR Grants Nos FA9550-07-1-0131 and FA9550-09-1-0004 monitored by Dr John Schmisseur.

References

[1] Roth J R, Sherman D M and Wilkinson S P 1998 Boundary layer flow control with a one atmosphere uniform glow discharge surface plasma *36th AIAA Aerospace Sciences Meeting and Exhibit* AIAA 98-0328
[2] Corke T C, Jumper E J, Post M L, Orlov D and McLaughlin T E 2002 Application of weakly-ionized plasmas as wing flow-control devices *40th AIAA Aerospace Sciences Meeting and Exhibit* AIAA-2002-350
[3] Benard N, Balcon N and Moreau E 2008 *J. Phys. D: Appl. Phys.* **41** 042002
[4] Glezer A and Amitay M 2002 *Annu. Rev. Fluid Mech.* **34** 503–29
[5] Roy S and Gaintonde D 2006 *Phys. Plasmas* **13** 023503
[6] Boeuf J P, Lagmich Y, Unfer Th, Callegari Th and Pitchford L C 2007 *J. Phys. D: Appl. Phys.* **40** 652–62
[7] Pinheiro M J 2006 *Plasma Process.Polym.* **3** 135–41
[8] Singh K P and Roy S 2008 *J. Appl. Phys.* **103** 013305
[9] Santhanakrishnan A and Jacob J D 2007 *J. Phys. D: Appl. Phys.* **40** 637–51